Nanodiamond Lateral Electron Emitter Devices

J.L. Davidson, W.P. Kang, and K. Subramanian
Department of Electrical Engineering & Computer Science, Vanderbilt University, USA

Introduction:

Diamond is an excellent material with unique properties such as low electron affinity and very high thermal conductivity suitable for electron field emission applications. Nanocrystalline diamond (henceforth, referred to as nanodiamond), possesses distinct properties including very small grain size, increased sp^2-carbon content, smoother surface morphology, and a wider latitude for materials integration, as well as the assets of the conventional CVD diamond. Planar lateral field emitters offer several advantages in high-speed and high-frequency applications with their simple fabrication process, design versatility of the electrodes' geometry, precise lithographic control of the inter-electrode spacing, and low capacitance features. Diamond lateral field emitters can be difficult to pattern, there being a scarcity of appropriate wet, dry, or plasma etching techniques for micron/submicron scale diamond patterning. We have developed multiple processes to micro-pattern diamond films by mold transferring technique[1] and topologically managed diamond vacuum field emitters, structured vertically[2-7] as well as laterally, including the first diamond lateral emitter[8]. In this work, we have developed a robust and reliable nanodiamond patterning technique using reactive ion etching (RIE) process and fabricated lateral diodes, which we will describe along with their field emission characteristics.

Experimental:

Nanodiamond films with grain size as small as 5 nm were achieved through the process of $CH_4/H_2/N_2$ microwave plasma enhanced chemical vapor deposition (MPECVD). One of the effective means to grow nanodiamond films is to increase the nucleation rate and decrease the growth rate by adjusting the CVD process parameters[9]. The nanodiamond growth process parameters employed were: flow rates of 15/8/190 sccm ($CH_4/H_2/N_2$), substrate temperature of 800 °C, microwave power and reactant pressure of 550 W and 20 Torr respectively, with a 0.1-0.2 μm/h growth rate. Figure 1 displays the SEM micrographs of these as-deposited nanodiamond films. The nanodiamond lateral field emitter devices were fabricated using a single-mask process. The process schema is shown in Figure 2. The fabrication begins with the growth of a 2-μm thick nanodiamond film on a silicon-on-insulator (SOI) wafer. Next, an aluminium metal layer was deposited and patterned with the lateral anode and cathode patterns using conventional photolithography. With this aluminum serving as a mask, patterning of the nanodiamond film was carried out with RIE in pure oxygen plasma using an *STS Advanced Oxide Etch (AOE^{TM})* ICP-RIE system, based on the inductively-coupled plasma technology. The coil R.F. power was 700W, while the platen R.F. power was 150 W, with the flow rate of oxygen being 30 sccm, at a pressure of 10 mTorr. Subsequent silicon etching was performed using the *STS Advanced Silicon Etch (ASE^{TM})* DRIE system in SF_6/O_2 (130 sccm/13 sccm) plasma at 600 W/12 W (coil/platen) R.F. power, and 21 mTorr pressure to achieve isolation between the nanodiamond electrodes and set the anode–cathode spacing. Figure 3 shows the structure of the nanodiamond lateral diode, with the patterned nanodiamond anode and cathode on the silicon layer; all on the SiO_2 layer on the silicon

substrate. Anode-cathode spacings were designed to be as low as 2 μm, which can enable the lateral device to operate at low voltages. The lateral field emission diode was characterized for field emission in a vacuum chamber at ~10^{-7} Torr (see schematic in figure 3).

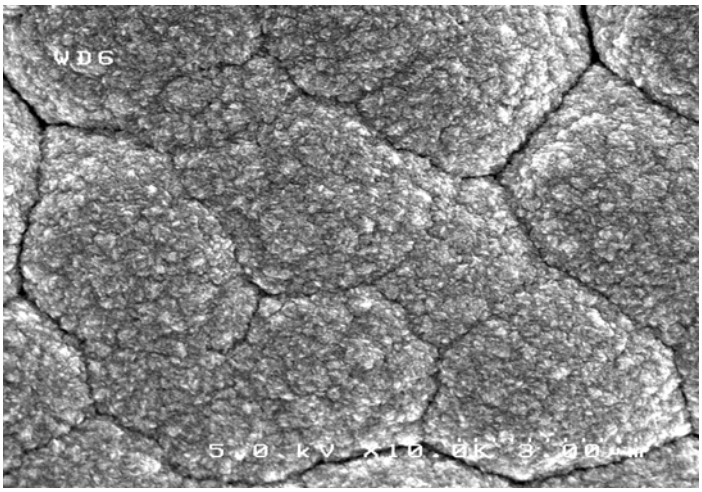

(a) 5.0 kV x 10.0 K 3.00 μm

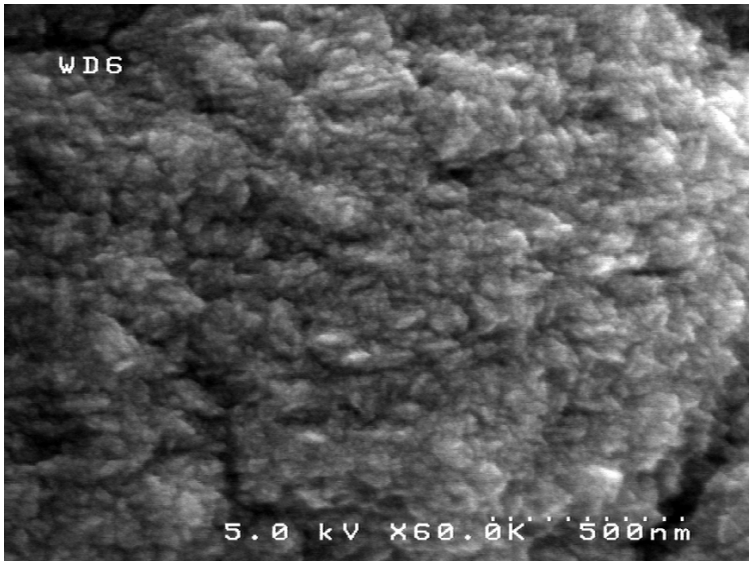

(b) 5.0 kV x 60.0 K 500 nm

Figure 1: SEM micrographs of as-deposited nanodiamond films by $CH_4/H_2/N_2$ MPECVD displayed at different magnifications.

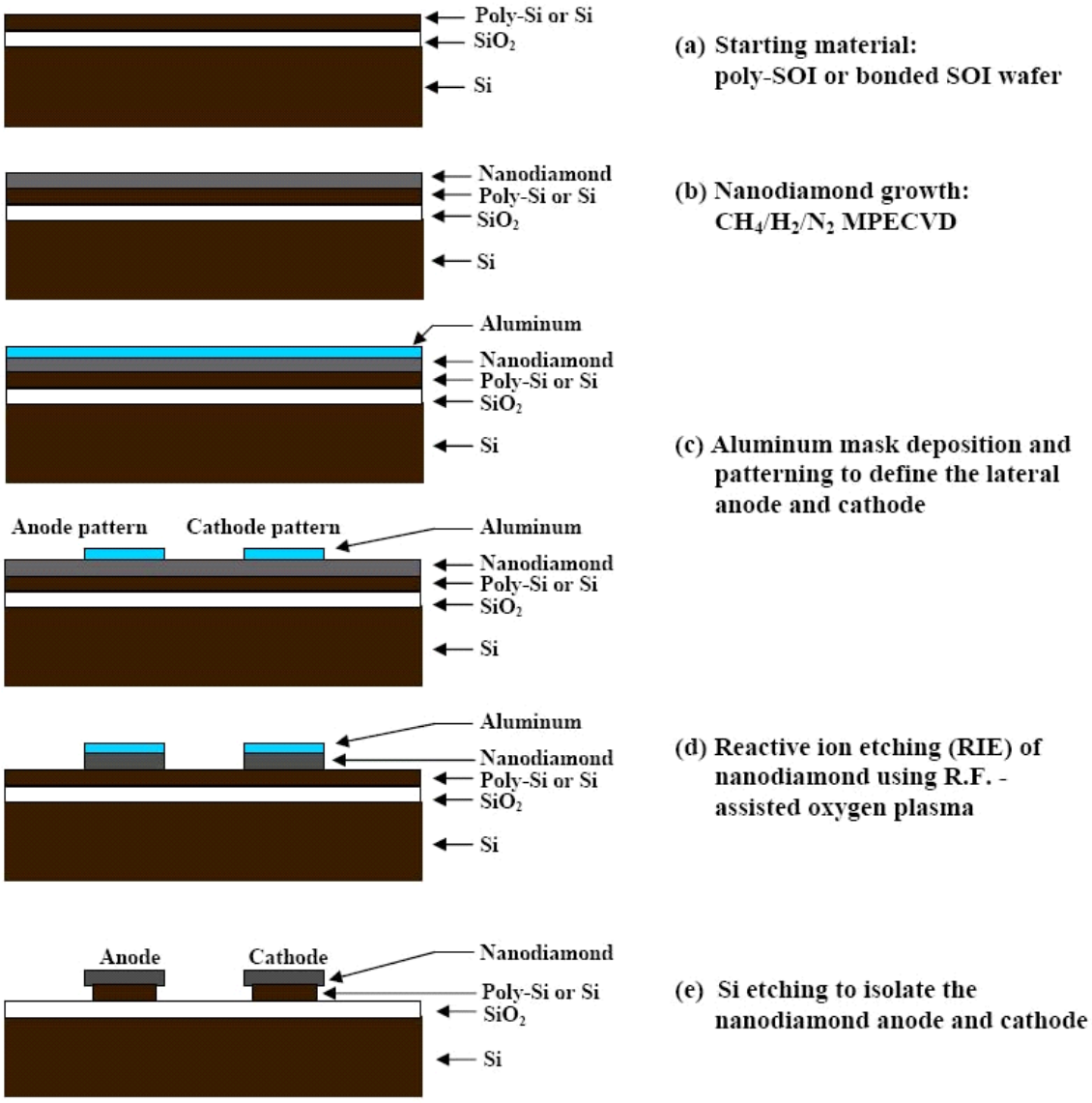

Figure 2: Fabrication process flow of the nanodiamond lateral field emission device

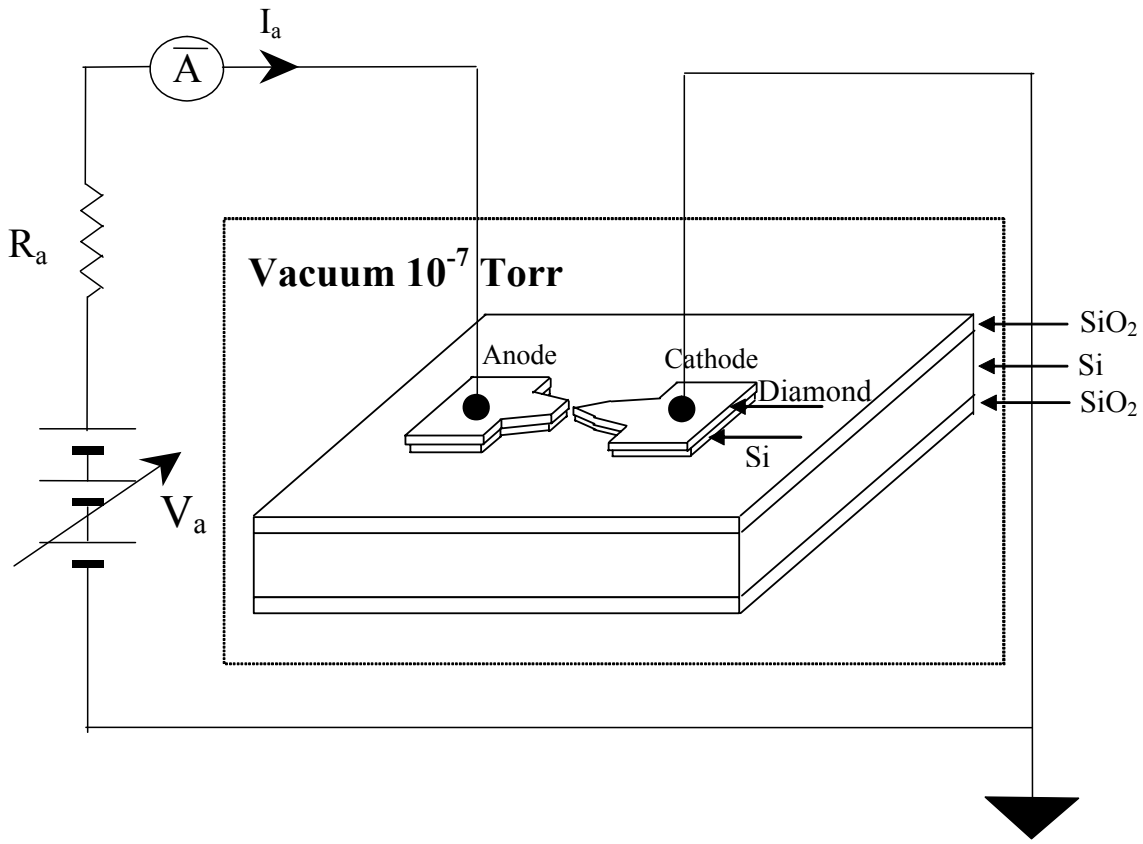

Figure 3: Field emission characterization set-up for the nanodiamond lateral diode

Results and discussion:

Arrays of nanodiamond lateral diodes were fabricated with anode-cathode distances ranging from 2 μm to 15 μm. Figure 4 shows the SEM micrographs of a 6-finger and 4-finger nanodiamond lateral diode with 4 μm anode-cathode spacing. The nanodiamond cathode has a high aspect-ratio finger-like emitter geometry with ultra-sharp apexes, which provides a geometrical field enhancement factor as compared to the nanodiamond anode, which has straight edge geometry. The lateral aspect ratio of each finger is ~3000 and ~4000 in specific cases. The 5 nm grain size of the nanodiamond film applied in the fabrication of the lateral device accounts for the ultra-small planar radius of curvature of the cathode fingers. The dielectric isolation layer in the lateral device is a 1 μm-thick SiO_2 layer, derived from the buried oxide layer of the SOI wafer. The advantage of using an SOI wafer in the fabrication of these lateral emitters is that the active Si layer of the wafer completely protects the SiO_2 layer beneath from any plasma-induced damage during the nanodiamond RIE process. Several other lateral devices from nanodiamond have been fabricated, with figure 5 displaying some of the different lateral emitter structures, batch-fabricated on the same chip using a single mask. The diamond patterning process employing the RIE offered high selectivity and yield. The diamond etch rate was found to be as high as ~ 0.5 μm/min. The aluminum mask was left with minimum damage after the RIE process, and thereby the anode and cathode were uniformly patterned to retain the strong field enhancement characteristics of the nanodiamond. Nanodiamond films provide a wider scope for micropatterning with their uniform top surface

morphology and small grain size, which aids optical lithography and uniform reactive ion etching.

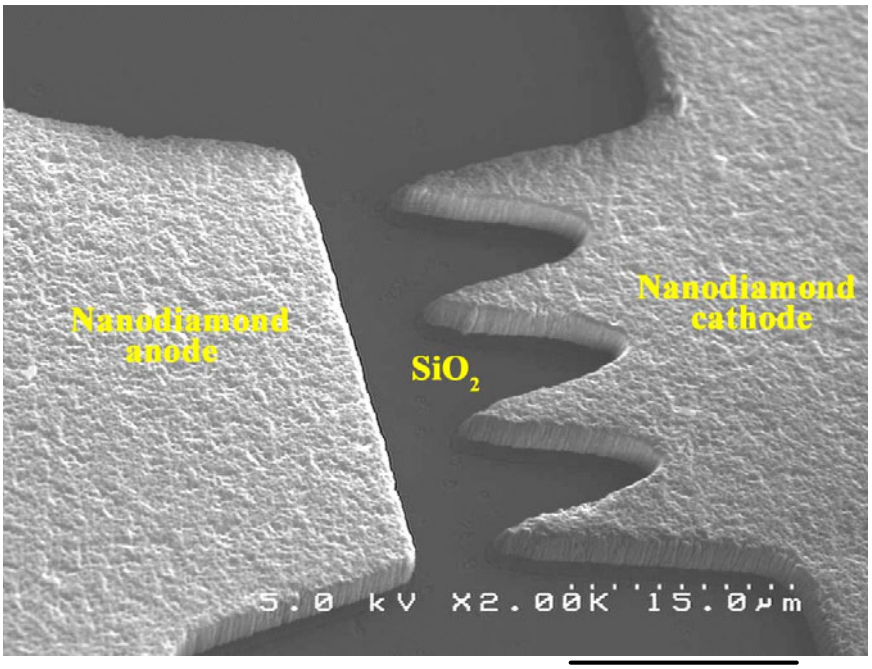

(a) 5.0 kV x 2.00 K 15.0 µm

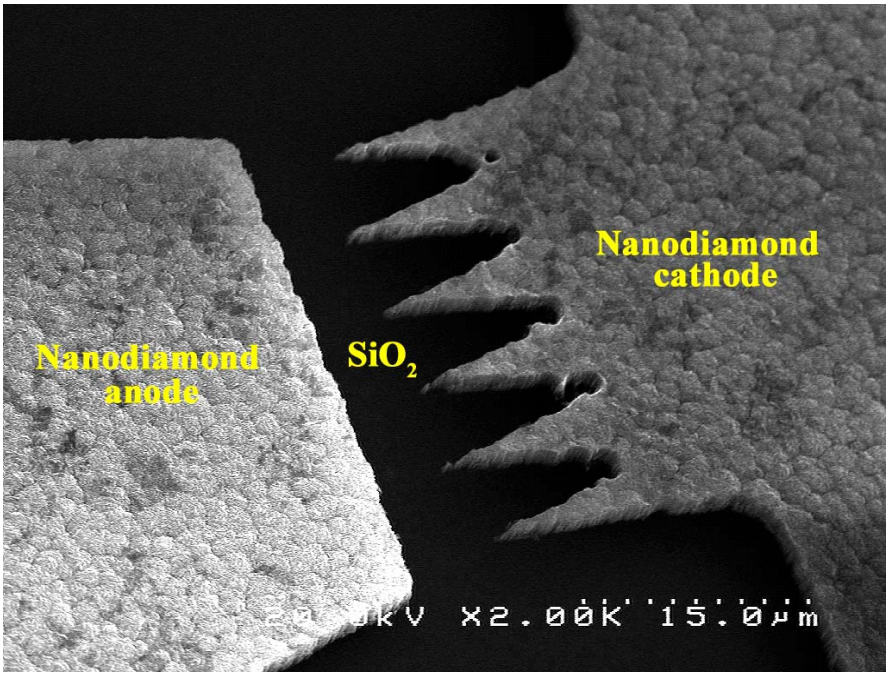

(b) 20.0 kV x 2.00 K 15.0 µm

Figure 4: SEM micrographs of (a) 4-finger nanodiamond lateral diode; (b) 6-finger nanodiamond lateral diode.

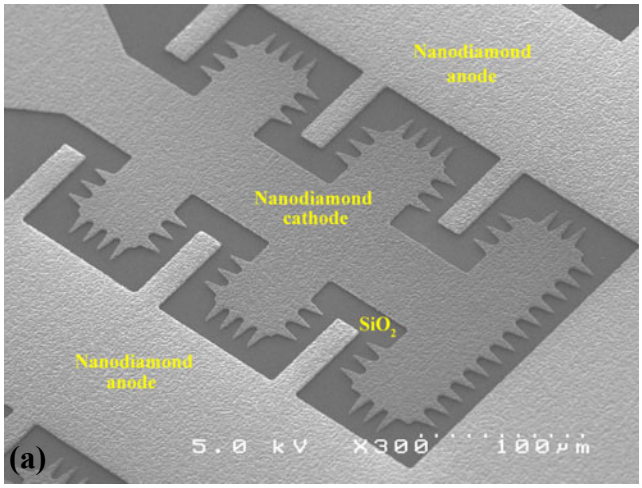

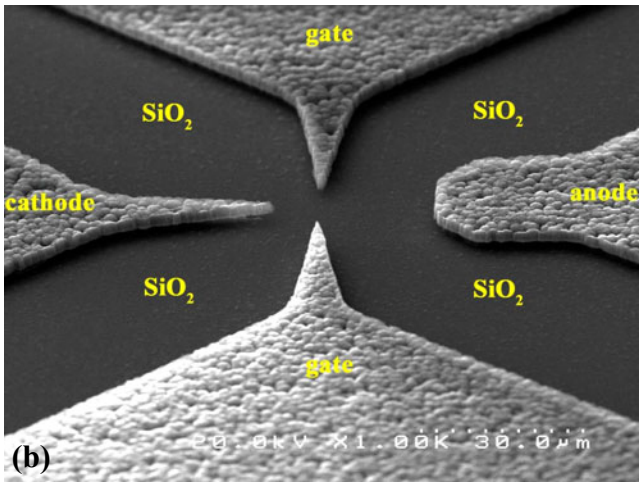

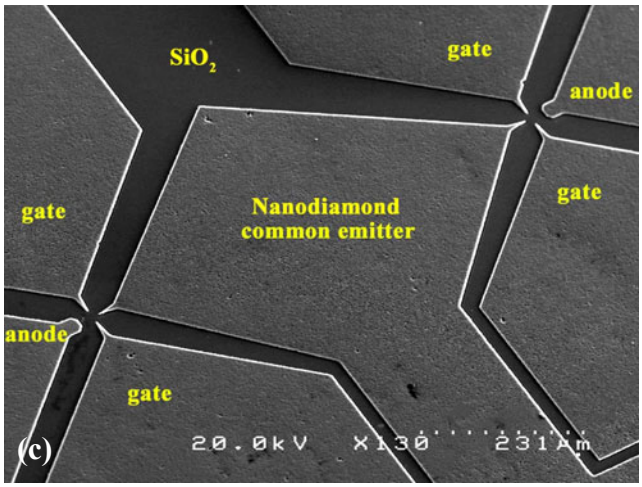

Figure 5: SEM micrographs of multiple lateral nanodiamond field emitter structures fabricated using a single mask: (a) comb-shaped emitter diode; (b) gated triode; (c) double triode with common emitter.

The nanodiamond 6-finger lateral diode with 3 µm anode-cathode spacing exhibited a low turn-on voltage of 5.9 V (electric field ~ 1.9 V/µm), which is one of the lowest reported for lateral field emission devices, and an emission current of ~ 5 µA at an anode voltage of 18 V (electric field ~ 6 V/µm). Figure 6 depicts the turn-on field emission characteristics of the device. The threshold current value used to determine a turn-on voltage is 10 nA per finger. The linear Fowler-Nordheim plot, as seen in the inset of figure 6, confirms that the observed current is attributed to field emission. The shallow slope of the FN indicates the presence of strong field enhancement factors in the nanodiamond fingered emitter.

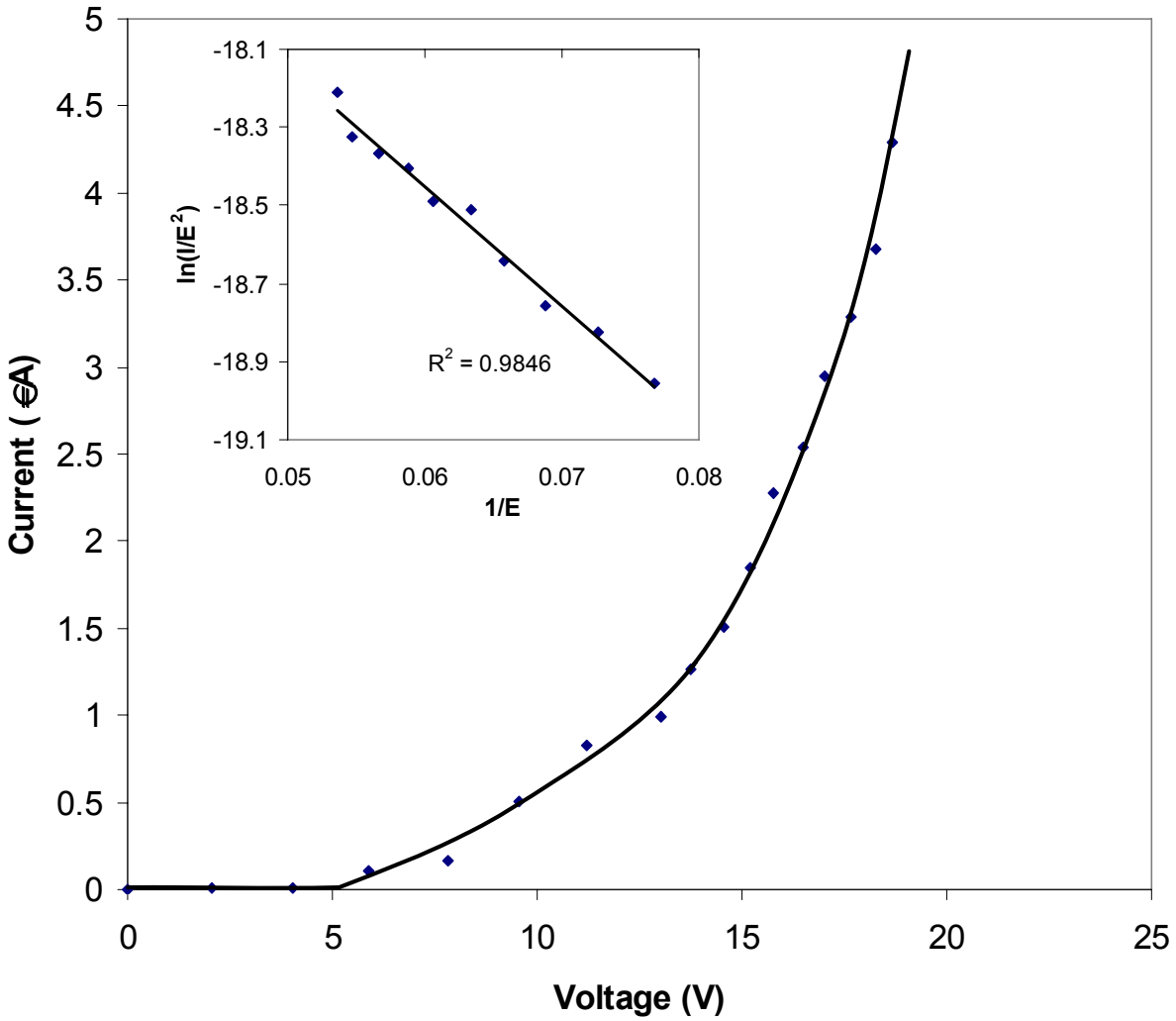

Figure 6: Threshold field emission characteristics of the 6-finger nanodiamond lateral diode.

The excellent emission characteristics of the nanodiamond lateral diode are attributable to its geometry with high aspect ratio and sharp apexes of the cathode fingers, increased sp^2-bonded carbon content in the nanodiamond, and nitrogen dopant incorporation in the diamond film. The effect of the geometrical field enhancement offered by the micropatterned finger-like emitter structures was determined using SIMION 7.0™ simulation software, whereby the lateral cathode and anode geometries were modeled and their equipotentials and electric field distributions were studied. The shape of the emitter geometries used for the equipotential line and electric field distribution calculations were exactly the same as that applied for the fabricated ones. The 6-fingered cathode emitter and the anode edge geometry were considered as the electrodes with an inter-electrode spacing of 5 μm. The potential arrays, defining the geometry and potentials of electrodes are utilized by *SIMION*[10]. The potentials of points outside electrodes are determined by solving the Laplace equation by finite difference

methods. Figure 7 shows the equipotential line plot of the lateral emitters in diode configuration for a given bias condition. The voltage to the edge geometry was set at 25 V, while the fingered geometry was grounded. The plot consists of 10 equipotential lines separated by 2.27 V each. The magnitude of the electric field at the very tip of each finger emitter and the corresponding edge-structured point is listed on the geometries, while the direction of the electric field is denoted by arrowhead. As one would expect, the electric field at the tip of the fingers is greater than that of the edge geometry throughout the device structure, indicating the enhanced field emission characteristics of the nanodiamond 6-fingered lateral emitters observed in vacuum.

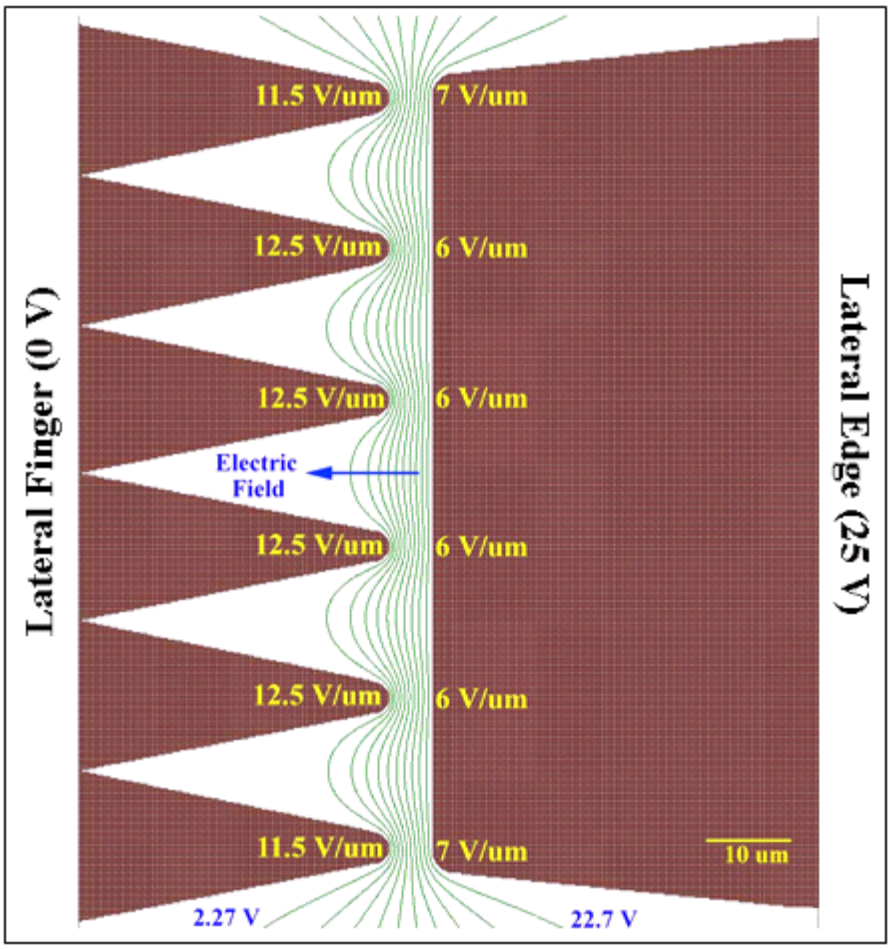

Figure 7: Equipotential line plot of the nanodiamond lateral field emitters in diode configuration at a given bias condition (lateral finger at 0 V & edge at 25 V), showing the magnitude and direction of the electric field of the chosen geometries.

Figure 8 shows the Raman spectrum of the nanodiamond film applied in the lateral device. The sp^3-bonded and sp^2-bonded carbon signatures are indicated by the peaks detected at 1332 cm^{-1} and 1580 cm^{-1} respectively. The ~1160 cm^{-1} peak in the spectrum indicates the nanocrystalline phase existing in the 5 nm grain-sized diamond film[11,12]. The sp^2/sp^3 peak ratio of the nanodiamond film was found to be ~0.97. Though the nanodiamond film possesses sp^2-carbon content, it should be noted that the scattering cross-section of sp^2-carbon is 50 times larger than that of sp^3-carbon, which confirms that the deposited film possesses a highly sp^3-bonded diamond structure. Electron transport in these diamond films have been discussed previously. Isolated conducting sp^2 nano-particles in the diamond film form a series of cascaded MIM (Metal-Insulator-Metal) microstructures, which enhance the electric field inside the diamond film and thereby increases the field enhancement factor. The enhanced electric field decreases the width of tunneling distance, at the metal-diamond interface significantly, and thereby increases the electron tunneling probability from metal into the conduction band of diamond. The electrons in the conduction band of diamond are then accelerated toward the next floating sp^2 particle under the induced electric field. Thus, the sp^2 particles would enhance diamond field emission[6,13,14]. The nanodiamond film grown by $CH_4/H_2/N_2$ CVD process possesses an increased sp^2-bonded carbon content because the nitrogen preferentially enters the grain boundaries, which are of increased volume density in the film, and promotes sp^2 bonding in the neighbouring carbon atoms[15].

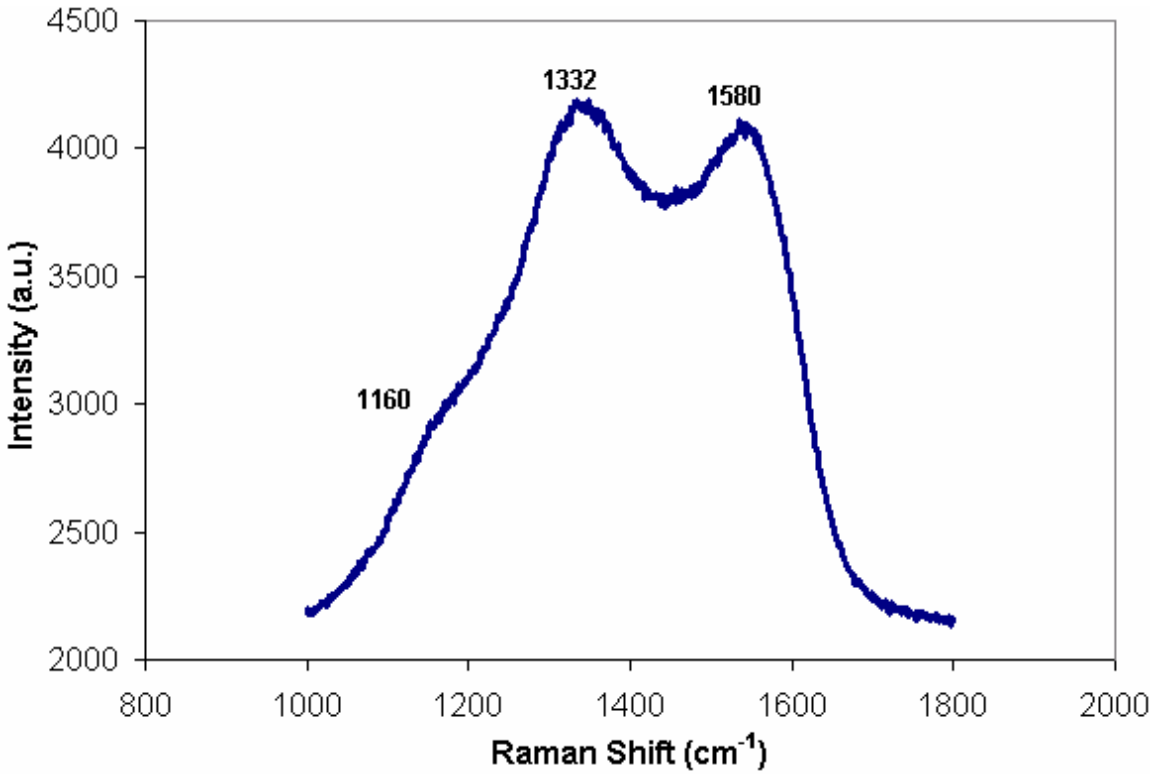

Figure 8: Raman spectrum of the as-deposited nanodiamond film ($CH_4/H_2/N_2$ MPECVD).

Energy dispersive spectrometry (EDS) x-ray microanalysis was used to characterize the chemical composition of the film. X-rays generated from the nanodiamond film under electron bombardment by the SEM were collected with a liquid nitrogen-cooled solid state Si (Li) detector and analyzed via computer according to their energy. Figure 9 represents the EDS spectrum of the nanodiamond film, displaying a real time histogram of X-ray count per channel versus energy expressed in KeV. The nanodiamond film profile exhibits the characteristic carbon and nitrogen elemental peaks at x-ray energies of 0.277 and 0.392 KeV respectively, indicating the incorporation of nitrogen in the diamond film. The nitrogen concentration increases the electrical conductivity of the diamond film, and can lead to the formation of deep donor levels, which raise the Fermi level and reduce the work function[12,16], thereby enhancing electron emission.

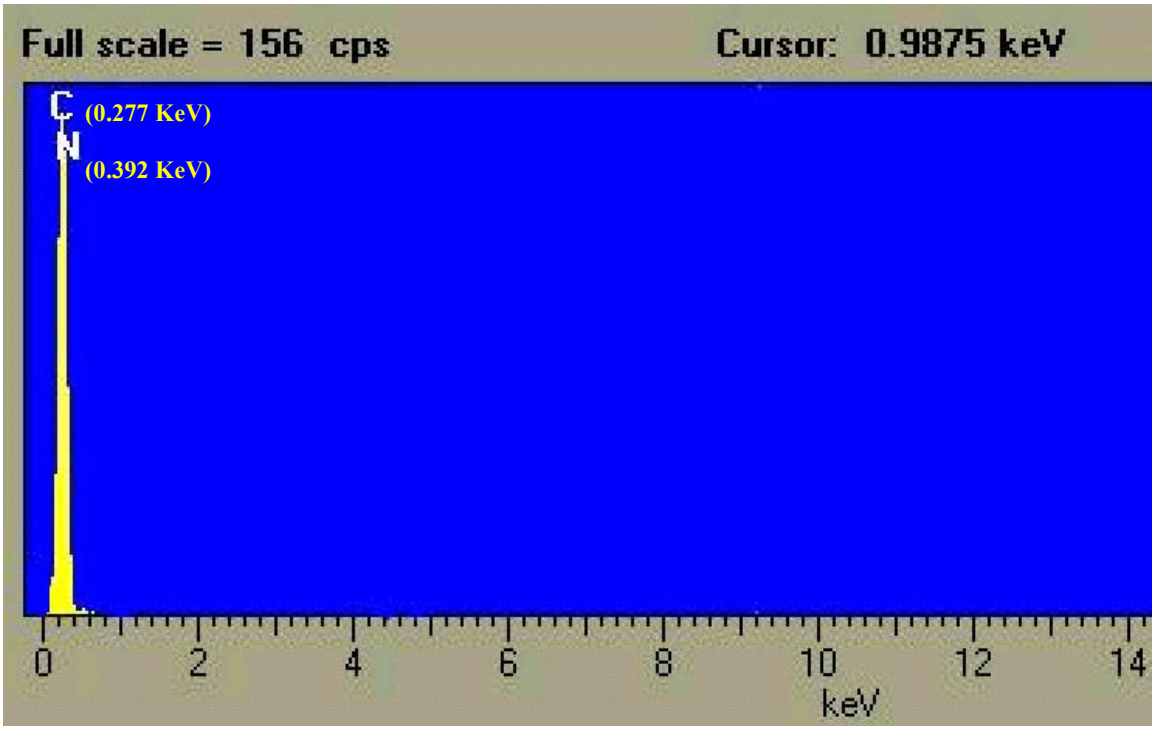

Figure 9: EDS x-ray microanalysis composition profile (X-ray count Vs Energy) of the nanodiamond film deposited by $CH_4/H_2/N_2$ MPECVD, indicating the incorporation of nitrogen impurity in the diamond film.

Conclusions:

A robust, well-controlled, and reliable process for the fabrication of nanodiamond planar lateral field emitters has been successfully developed. A very small anode-cathode spacing and versatile diamond emitter configurations have been achieved. The 6-finger lateral diode, thus fabricated by applying nanodiamond grown by $CH_4/H_2/N_2$ MPECVD, possesses favourable properties, viz., 5 nm grain size, smooth surface morphology, increased sp^2-carbon content,

and nitrogen dopant concentration, subsequently demonstrates excellent field emission characteristics. These lateral field emitters find potential applications in high speed, high frequency, and high power applications, due to their low voltage operation, brought about by their micron/submicron anode-cathode spacing. The lateral nanodiamond field emitter structure microfabrication technique, based on its single-mask utility, high manufacturability, combined with its reproducibility, is a very efficient and low-cost approach to realize practical electron field emitters.

References:

[1] W. P. Kang, J. L. Davidson, and D. V. Kerns Jr., *United States Patent Number: 6,132,278*, (2000 October 17).
[2] W.P. Kang, J.L. Davidson, A. Wisitsora-at, Y.M. Wong, R. Takalkar, K. Holmes, and D.V. Kerns, *Diamond and Related Materials 13,* 1944 *(2004)*.
[3] A. Wisitsora-at, W. P. Kang, J. L. Davidson, D. V. Kerns, and T. Fisher, *Proceedings of the 14th International Vacuum Microelectronics Conference, Davis, CA.,* 285 (2001).
[4] A. Wisitsora-at, W. P. Kang, J. L. Davidson, D. V. Kerns, and S. E. Kerns, *13th International Vacuum Microelectronics Conference, Guangzhou, China,* 136 (2000).
[5] W. P. Kang, A. Wisitsora-at, J. L. Davidson, M. Howell, D.V. Kerns, and F. Xu, *J. Vac. Sci. Technol. B 17,* 740 (1999).
[6] W.P. Kang, A. Wisitsora-at, J.L. Davidson, D.V. Kerns, Q. Li, J. F. Xu, C. K. Kim, *J. Vac. Sci. Technol. B 16* , 684 (1998) .
[7] A. Wisitsora-at, W. P. Kang, J. L. Davidson, and D.V. Kerns, *Appl.Phys.Lett.71,* 3394 (1997).
[8] W. P. Kang, J. L. Davidson, A. Wisitsora-at, M. Howell, A. Jamaludin, Y.M. Wong, K.L. Soh, and D.V. Kerns, *J. Vac. Sci, Technol. B 21,* 593 (2003).
[9] K. Subramanian, W.P. Kang, J.L. Davidson and W.H. Hofmeister, *Diamond and Related Materials 14*, 404 (2005).
[10] D.A. Dahl, *SIMION 3D Version 7.0 User's Manual,* 2-5 (2000).
[11] M. Stammler et al., *Diamond and Related Materials 8*, 792 (1999).
[12] S.G. Wang, Qing Zhang , S.F. Yoon , J. Ahn , Q. Zhou , Q. Wang , D.J. Yang , J.Q. Li , Sam Zhang Shanyong, *Surface and Coatings Technology 167,* 143 (2003).
[13] Wisitsorat-at, Anurat, *Ph.D. Dissertation,* Electrical Engineering, Vanderbilt University, USA,114 (2002).
[14] A. Wisitsora-at, W. P. Kang, J. L. Davidson, Y. Gurbuz and D. V. Kerns, *Diamond and Related Materials 8* , 1220 (1999) .
[15] T.D. Corrigan, D.M. Gruen, A. R. Krauss, P. Zapol, R. P. H. Chang, *Diamond and Related Materials 11*, 43 (2002) .
[16] S. Bhattacharyya, O. Auciello, J. Birrell, J.A. Carlisle, et al., *Appl.Phy.Lett. 79, No. 10,* 1441 (2001).